Biofouling
Vol. 25, No. 5, July 2009, 445–454

Taylor & Francis
Taylor & Francis Group

Impact of wastewater fouling on contact angle

Evan Thomas* and Dean Muirhead

NASA-Johnson Space Center, Mailcode EC3, 2101 NASA Parkway, Houston, TX 77058, USA

(*Received 19 November 2008; final version received 7 March 2009*)

Capillary dependent systems are highly influenced by surface fouling and may degrade as material surface properties change. In anticipation of a spacecraft microgravity fluids management system exposed to highly variable wetting conditions, the impact of urine wastewater fouling on capillary contact angle was examined. The results indicate that, in general, surface fouling can decrease the contact angle when crystalline structures or biofilms form. Small crystalline growth on the order of 10 μm can lower advancing contact angles θ_{adv} by approximately 30°, while biofilm growth can lower it by approximately 15°. Vacuum drying of fouled surfaces increased θ_{adv} by about 8°, and defects greater in height than 5% of the capillary length increased θ_{adv} by approximately 30°. These trends may indicate that promotion of wastewater fouling may improve the performance of capillary dependent fluids management systems. These results may also influence terrestrial technologies, including medical catheters and sustainable wastewater treatment systems exposed to wastewater fouling.

Keywords: wastewater fouling; microgravity fluids management; advancing contact angle; wetting; urine

Introduction

The contact angle θ is a key design parameter for capillary-based liquid management systems. A hydrophilic system consists of a liquid with more affinity for an adjacent solid surface than for itself. In a hydrophobic system, the liquid has more affinity for itself than for the solid surface. Capillary systems can be designed for a range of contact angles based on the selected materials and liquids. The three general wetting regimes include spreading, partial wetting, and non-wetting, and are characterized primarily by the contact angle. In many wetting systems, spontaneous capillary driven flows arise as a natural consequence of the system geometry. This is known as capillary action (Dodge 2000). Capillary systems often consider advancing contact angles θ_{adv} that are observed on liquids moving across surfaces. Lower advancing contact angles generally produce better performing capillary systems.

In this study, the impact of wastewater fouling on contact angle was characterized in support of the development of a microgravity fluids management system called the Static Phase Separator (SPS). This technology is described in Weislogel et al. (2008). The SPS is designed without moving mechanical parts to separate urine and air. It uses only fluid momentum and capillary action. The performance of the system is highly dependent on the wetting characteristics of the liquid and solid materials. The system is novel in that capillary driven systems are normally designed for known and favorable wetting conditions. Instead, the SPS is designed for highly variable and potentially unfavorable wetting conditions. For this study, the urine fouling of solid surfaces was evaluated on the basis of changing contact angle. The results have applicability to other microgravity and terrestrial fluids management systems. Applications include medical catheters exposed to urine fouling, sustainable wastewater management systems that utilize wastewater wetting, and laboratory-on-a-chip applications examining highly variable aqueous solutions. This study provides a background for the surface properties of wastewater fouling layers on solid surfaces.

Materials and methods

This work was application driven. The objective was to evaluate contact angle changes due to a variety of fouling conditions. The scope of the experiment was not concerned with specific cause and effect of wastewater fouling, but rather with the general trends of fouling on wetting characteristics quantified by contact angle measurements. Wastewater fouling tests were used to condition solid coupons for contact angle measurements. During subsequent analysis, the data were grouped by fouling layer characteristics.

Three types of solid materials were used in this study: polished Titanium-64 (hydrophilic), polished

*Corresponding author. Email: evan.a.thomas@nasa.gov

ISSN 0892-7014 print/ISSN 1029-2454 online

DOI: 10.1080/08927010902875105
http://www.informaworld.com

Aluminum-7075 (hydrophilic), and smooth Ultem (hydrophobic). These materials were selected for their surface energy properties, potential fouling characteristics, and as common aerospace materials. The materials were cut into coupons approximately 5 cm by 7 cm, in a similar manner to those of previous studies (Brizzolara and Holm 2006; Simoes et al. 2007).

Apparatus design

An apparatus was employed to circulate air and urine over solid coupons simulating the three-phase interactions expected for the target SPS application. The apparatus is shown in Figure 1. The coupons are $\sim$70% submerged in the liquid at a 20° angle from vertical. ColeParmer peristaltic pumps were used to circulate the wastewater and laboratory air through the apparatus. All tests were conducted with a liquid flowrate of 300 ml min^{-1} and an air flowrate of 1800 ml min^{-1} at $\approx$20°C.

For the apparatus it was assumed that extensive biofouling and crystal formation is achieved primarily as a result of the turbulent, well mixed flow. Turbulent conditions result in bacterial cells having more frequent association with the solid surface and thereby increased likelihood of attachment (Donlan 2002). While biofilms have been demonstrated to be more substantial in turbulent flows, the cells within those biofilms are less active than those in laminar conditions (Simoes et al. 2007). In turbulent flows, there is likely an increase in the production of the biofilm matrix, making the biofilm more adhesive (Oliveira 1992).

Wastewater test conditions

The wastewater used in this study was primarily urine composite from several human male and female donors. The test conditions are summarized in Table 1. Tests T1 through T6 used one coupon of each material, whereas tests T7 through T11 used one coupon of titanium. Tests T1 through T8 used 225 ml batch sizes. Test T9 used machined titanium blades instead of polished coupons, and a particular loading to be described shortly. Tests T10 and T11 used 160 ml batch sizes. The tests ranged in duration from 7 to 180 days, with wetting times ranging from 2.5 to 180 days. Except for T9, the same urine batch was used throughout each test.

Wetting and drying durations were not rigorously controlled since the main objective was to create a variety of fouling layers and not conduct a detailed investigation on the formation mechanisms of such layers.

For five of the eleven tests, the urine was pretreated with a standard 5 g l^{-1} dose of Dupont Oxone (predominately potassium monopersulfate), an oxidizing and disinfecting compound used by NASA for urine pretreatment aboard spacecraft. The pretreatment is designed to lower the pH of the urine to as low as 3 and prevent bacterial growth from proliferating and producing the enzyme urease which contributes to the formation of ammonia gas and ammonium through the hydrolysis of urea (Winkler et al. 1983). The hydrolysis process raises the pH of the urine, which reacts with other chemicals in the urine to form precipitates, primarily struvite (Doyle and Parsons 2002). Turbidity increases because of bacterial growth, crystal formation, and precipitation. All of these processes pose potential problems to wastewater management systems (Wallace and Campbell 2005).

For several tests, the urine was seeded with urine acclimated bacteria to simulate extensive and accelerated bacterially induced fouling. Bacterial activity was measured by heterotrophic plate count (HPC) in colony forming units (CFU ml^{-1}). Fresh untreated

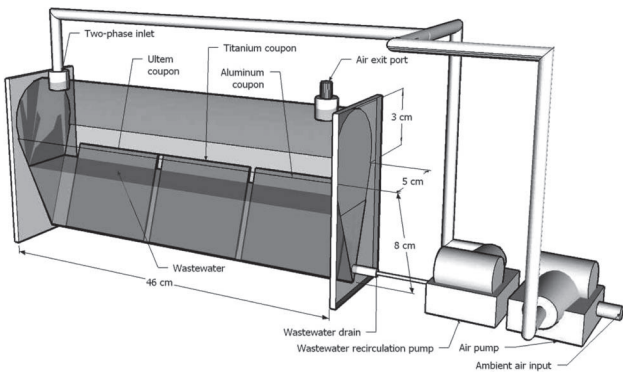

Figure 1. Apparatus diagram.

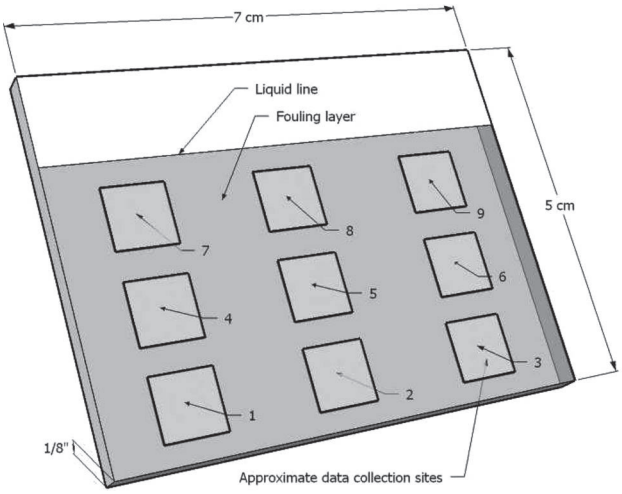

Figure 2. Coupon analysis points.

Table 1. Coupon fouling layer conditioning tests.

Test	Wastewater conditions	Wetted time (days)	Total duration (days)	HPC pre/post (CFU ml^{-1})
T1	Urine composite, pretreated 5 g l^{-1} Oxone	2.51	9.15	0 –
T2	Urine composite, untreated	7.75	14.04	90 $2(10)^8$
T3	50% urine composite, 50% MBC, untreated	8.71	14.29	$2(10)^7$ $2(10)^8$
T4	50% urine composite, 50% MBC, pretreated 5 g l^{-1} Oxone	15.79	18.92	0 $1.3(10)^8$
T5	50% urine composite, 50% MBC, pretreated 5 g l^{-1} Oxone	6.67	7.08	16 $1(10)^7$
T6	75% urine composite, 25% MBC, pretreated 5 g l^{-1} Oxone	6.35	7.96	0 0
T7	Urine composite with calcium and oxalate	4.98	8.15	24 $3.6(10)^8$
T8	Urine composite with egg albumin protein	3.56	6.75	20 $5.8(10)^8$
T9	Fresh urine composite each day untreated	Representative use, see text		$2.5(10)^7$ $1.55(10)^8$
T10	Urine composite, untreated	Stagnant	180 days	$2(10)^7$ $1(10)^5$
T11	Urine composite, pretreated 5 g l^{-1} oxone	Stagnant	180 days	0 0

urine ranges in bacterial activity from tens to tens of millions of CFU ml^{-1}, depending on the dermal and atmospheric bacteria collected. The seeding process mixed aged urine with high bacterial concentrations (typically about 10^9 CFU ml^{-1}) and high pH (above 8.0, a characteristic of urea hydrolysis) with fresh urine to ensure that urease producing bacteria was introduced to the fresh urine composite. This seeding source is called the microbiological consortium (MBC), which is prepared by mixing aging urine with fresh urine over several days, and monitoring for increases in total ammonia nitrogen and pH, both of which are indicators of urea hydrolysis.

In test T7, untreated urine composite was loaded with calcium chloride and potassium oxalate to simulate the calcium and oxalate offloading experienced by astronauts during spaceflight due to bone atrophy. This test attempted to simulate extensive calcium oxalate crystal fouling based on flight data (Whitson et al. 1997, 2001), adding 300 mg l^{-1} calcium and 50 mg l^{-1} to the urine composite in the form of calcium chloride and potassium oxalate. Test T8 aimed to examine worst case urine foaming. Urine foaming is caused by protein surfactants and may impact fouling and wetting conditions. A major constituent of urine protein is albumin. Albumin concentration in urine can vary greatly between individuals but in general ranges from 90 to >300 mg l^{-1} (Comper et al. 2004). Therefore, for T8, 300 mg l^{-1} of egg albumin (Fisher Scientific S93108) were added to approximate high urine albumin concentrations.

T9 simulated the conditions that the target application, the SPS, would experience in spaceflight. This test used a sub-scale test article of the SPS with conditions selected to simulate requirements for the waste management system in the current NASA architecture (NASA-JSC 2008). The test article was run continuously for 21.1 days, filling one-third of the article 36 times per day. The test article and fluid lines were cleaned with 200 proof ethanol, and sealed with silicone rubber. The influent polycarbonate laboratory bottle was cleaned each day with hot water and filled with fresh untreated urine composite. The effluent polycarbonate laboratory bottle was drained and rinsed every day. Each batch of urine flowed for 24 h in a single pass, except for on one occasion where a single batch was re-circulated for a second 24 h period. In a supporting experiment conducted by the authors, fresh urine in sterile containers did not show a significant increase in pH or total ammonia nitrogen for at least 7 days, indicating little production of urease producing bacteria. Therefore, the microbiological activity and precipitate growth on the surface is dominated by activity within the growing fouling layer, rather than extensive microbiological activity in the liquid phase. Using re-circulated urine for up to 48 h was not anticipated to have a significant effect.

Tests T10 and T11 in part simulated the expected non-use period for the orbiting system. The urine used for both tests was taken from the same composite sample. Test T10 remained untreated while test T11

was pretreated with 5 g l^{-1} Oxone. A 160 ml sample of each was contained in bottles with 50% by volume headspace for 180 days.

Fouling analysis

A variety of diagnostics were employed to analyze the nature and extent of the solid coupon fouling at the end of each test. The fouling of interest includes biofouling, mineral scaling, corrosion, and foaming. Quantitative and qualitative data were collected both in the liquid phase and on the solid surface of the test coupons for each test. Figure 2 is a sketch of a test coupon with the approximate locations on the coupon used for the analysis.

At points 3, 5, 7 (Figure 2), an FEI XL30 environmental scanning electron microscope (ESEM) was used to image the solid coupons at 250×, 500×, and 2000× magnifications, and a Keyence VHX digital microscope was used to take three-dimensional surface images of the fouled coupons. A Bruker Tensor 27 Fourier transform infrared (FTIR) microscope was used to obtain infrared spectra for identification of biofilm presence. A Metrohm 850 Professional Ion Chromatograph was employed to determine the liquid phase ion concentrations using manufacturer methods (Metrohm 2008), and a traditional suite of instruments were applied to characterize the liquid phase of the test using Standard Methods for the Examination of Water and Wastewater (APHA 2006), including turbidity (2130B), conductivity (2510B), temperature (2550B), pH (4500-H + B), dissolved oxygen (4500-O G), and HPC (9215B).

Figure 3 provides a representative ESEM image. In this case, the coupon was exposed to stagnant Oxone-pretreated urine for 180 days. Such images reveal a high density of crystalline growth over the entire surface (100% coverage in this case).

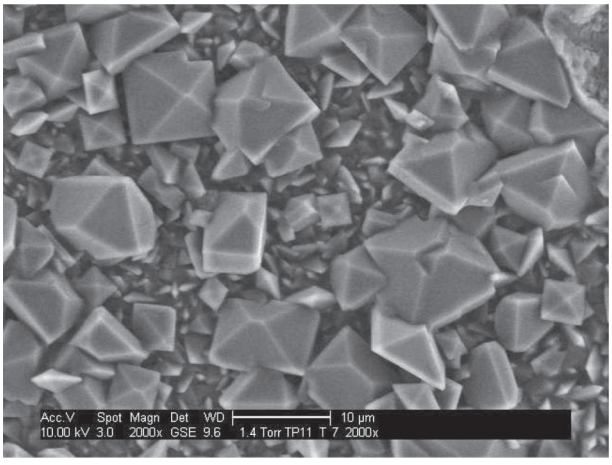

Figure 3. T11 ESEM image.

Providing a direct measure of surface wettability, advancing contact angle data θ_{adv} were collected using a Dataphysics Optical Contact Angle 15 (OCA 15) Goniometer and the sessile drop method with deionized (DI) water on the fouled coupon surfaces. Contact angle measurements were taken at three separate locations on each of the coupons. There was no influence anticipated on a chemical level when using DI water to measure contact angle *vs.* urine of a different pH, as contact angle measurements take only seconds, while crystal induction time requires days. DI water was used for contact angle measurements in this experiment for consistency in liquid surface tension. A parallel experiment indicates that over a variety of urine types on five different materials, urine contact angles were significantly lower ($p = 0.046$) than DI water contact angles on average 9.8° with a 95% confidence interval of 0.3° to 19.3°. It was expected that urine θ_{adv} would almost always be lower than DI water values.

Results, analysis, and discussion

Several statistical methods were used to analyze the data, including two-sample unpaired and paired *t*-tests and linear regressions. A significance level α of 0.05 is chosen. All data sub-sets pass tests for normality and homogeneity of variance. The statistical analysis was not concerned with the direct dependence of the test conditions on the fouling layer constituents, rather the general impact of fouling layer conditions on contact angle. Therefore, rather than an intricate analysis of variance with multiple variables, the impact of fouling layer characteristics on contact angle were evaluated by correlations and mean differences of contact angles for several characteristic groups. The data in each analysis were a subset of all the data collected and were grouped such that the particular parameter of interest could be best evaluated for impact on contact angle.

The baseline DI water on titanium θ_{adv} used in the data set was 69.7° ± 2.7°, which was collected during extensive urine and water contact angle measurements across seven clean materials. This baseline is consistent with other measurements and lower than urine on visibly clean and smooth titanium, which is around 77°.

The dataset included 147 θ_{adv} measurements. The results were grouped to isolate fouling trends. Only the significant characteristics identified are presented. ESEM, FTIR, and VHX data were matched to θ_{adv} measurements taken at approximately equivalent liquid flow levels on the coupons. For example, an ESEM areal coverage determination at point 3 on a given coupon was matched to contact angle measurements on points 1 and 2 (Figure 2). This approach assumed similar fouling across the same liquid flow path.

The most significant results are distilled and listed in Table 2 and presented graphically in Figure 4, both of which reflect the trends of the influences of these fouling characteristics on θ_{adv}. These results do not presume rigorous isolation of fouling constituents, but rather provide insight for engineering applications. For example, observation of Table 2 and Figure 4 show the degree to which fouling characteristics like crystal and biofilm growth serve to improve wetting, while other parameters like vacuum drying and large defects serve to reduce wetting. Each of these impacts will be discussed in turn.

Impact of material selection

Because the coupons in each test were exposed to identical conditions, a two-sample paired *t*-test was conducted to determine the impact on θ_{adv} between materials. The test conditions produced layers that completely cover the solid surfaces resulting in no significant difference in contact angle between material groups. This is not to say that material selection is not important in design, but rather that when extensive fouling is present the influence of the substratum material is insignificant on θ_{adv}.

Impact of vacuum drying

Two sets of contact angle measurements were made on each coupon. The first measurements $\theta_{adv}A$ were collected at points 1, 6, and 8 (Figure 2) shortly after the coupons were removed from the test apparatus and allowed to air dry. The second measurements $\theta_{adv}B$ were collected at points 2, 4, and 9 after the coupons were allowed to vacuum dry in the ESEM. Each θ_{adv} data point was the mean of at least 2, and on average 6, θ_{adv} values measured for an advancing drop at a given location on the coupon with a SD $< 2^{\circ}$.

A linear correlation test was applied to $\theta_{adv}A$ and $\theta_{adv}B$ and showed a significant probability correlation ($p = 2^{-11}$) when all data were considered for each test location. Operator error, instrument, laboratory methods, and a Matlab θ_{adv} reduction algorithm all contribute errors. However, because the measurements of $\theta_{adv}A$ and $\theta_{adv}B$ were taken on separate days and there remains a significant correlation, it can be concluded that the errors do not significantly affect the validity of the θ_{adv} data.

A two-sample paired *t*-test was performed on the data for the influence of ESEM vacuum drying. The results indicate that vacuum drying had significant influence ($p = 0.0028$) on contact angle and increased θ_{adv} by approximately 3° to 13°. This increase is likely due to contact line pinning. The initial θ_{adv} results are obtained on air-dried coupons that did not contain any obvious moisture. After the coupons were vacuum dried in the ESEM, the crystalline and biofilm surfaces were roughened by cracking. This produced an increase in pinning edges and a subsequent increase in θ_{adv} as described by Dyson (1988).

Impact of biofilm growth deposits

Non-destructive FTIR was selected to identify the presence or absence of biofilm growth. Only one study to the authors' knowledge has extensively discussed the application of FTIR to wastewater fouling (Schmitt and Flemming 1998). FTIR reflectance spectra were collected using a Bruker Tensor 27 FTIR-Spectrometer. The biofilm spectral features were

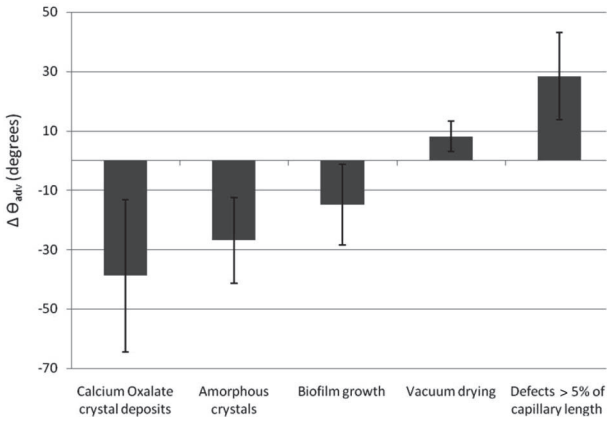

Figure 4. Impact of surface fouling conditions on $\Delta\ \theta_{adv}$ with 95% confidence intervals.

Table 2. θ_{adv} (°) as a function of surface fouling conditions.

Parameter	Sample size	Absence (°)	Presence (°)	*p*-value	95% confidence interval (°)	
Calcium oxalate deposits	36	20.5	59.3	0.0042	13.1	64.4
Magnesium influenced amorphous crystals	27	72.1	45.2	0.0007	12.5	41.3
Isolated biofilm growth	54	74.7	59.8	0.034	1.2	28.5
Vacuum drying	69	53.9	62.0	0.0028	3.0	13.3
Defect heights >5% of capillary length	66	44.3	72.7	0.0003	13.7	43.1

interrogated in the fashion of Schmitt and Flemming (1998). Other fouling layer constituents have overlapping spectral peaks, so several distinct biofilm spectral peaks were required to conclude biofilm presence. A representative chart of this process is shown in Figure 5, where the top three spectra are from T5 and the bottom three from T6. As shown, the T6 spectra show distinct biofilm constituent peaks. While the extent and nature of biofilm growth was not quantified, the occurrence of biofilm growth is expected to be sufficient to determine an influence on contact angle.

The presence or absence of biofilm growth was isolated from small crystal growth by selecting data that showed biofilm growth in the absence of crystal growth. This analysis indicated that biofilm alone can significantly decrease ($p = 0.034$) θ_{adv} by approximately 1° to 28°. The presence or absence of biofilm in turn had a statistically significant impact on the overall coverage of the coupons by the fouling layer. On the 500× images, which have the most significant correlation ($p = 0.016$) of the three magnifications, the presence of biofilm increased the fouling coverage by approximately 30%.

Biofilms are known to be porous when dried (Donlan 2002) and adsorption is known to be a critical factor in θ_{adv} measurements (Sharma and Hanumantha 2002). The biofilm matrix is highly hydrated when exposed to bulk liquid, with water accounting for over 98% of the biofilm matrix mass (Cooksey 1992). The biofilm matrix is known to be hygroscopic (Fletcher 1992; Schneider et al. 2005), and therefore water sorption will occur when the hygroscopic biofilm surfaces are dried and then re-exposed to water based liquids. For a hygroscopic substance the decreased θ_{adv} observed is consistent with hygroscopic surfaces being known to be spontaneously invaded when wetted (Bico et al. 2001).

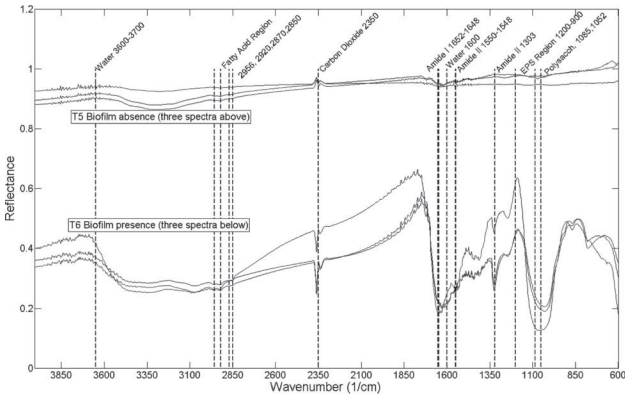

Figure 5. T5, T6 representative FTIR spectra with biofilm peaks.

Impact of crystal deposits

The ESEM images were used to determine the type of crystalline deposits on the coupons. Visual comparison of the crystals to known urine crystal geometries is an established method as demonstrated in previous investigations (Strasinger and DiLorenzo 2001; Brunzel 2004). When pH is a factor in identifying crystal types, visually similar crystal types are grouped. The crystals identified on the fouled coupons include calcium oxalate, struvite, and either uric acid or calcium phosphate. These were treated as a group because of their similar appearance.

The dataset for titanium coupons was categorized by the presence and absence of clearly defined calcium oxalate deposits. The analysis indicated that the presence of calcium oxalate deposits significantly decreased ($p = 0.0042$) θ_{adv} by approximately 13° to 64°.

The initial concentration of magnesium in the liquid phase (Pre Mg) had the most significant correlation to θ_{adv} of any parameter. An average concentration of magnesium was assumed for analysis with test T9, which used 21 different urine composite samples. The concentration of magnesium in the liquid phase is often the limiting ion for struvite precipitation (Udert et al. 2003). However, the presence of struvite crystals does not significantly alter θ_{adv} or Pre Mg. Instead of defined struvite deposits impacting θ_{adv}, it is likely that uric acid or phosphate deposits, including magnesium urates and phosphates, were the surface deposits influenced by Pre Mg that impact θ_{adv}. Uric acids and phosphates can precipitate in amorphous forms. These precipitates can include sodium, potassium, magnesium and calcium urates or phosphates, and appear as small grains (Strasinger and DiLorenzo 2001; Brunzel 2004). The presence of amorphous crystals excluding calcium oxalates was statistically correlated to the initial concentration of magnesium, with the absence of amorphous crystals indicating a lower initial concentration of magnesium. The presence of amorphous crystals, influenced by magnesium concentration, significantly lowered ($p = 0.0007$) θ_{adv} by approximately 12° to 41°.

Calcium and oxalates were added to the urine composite in test T7 to promote calcium oxalate fouling, but did not show defined calcium oxalate crystals. The T7 test liquid phase was used for over 8 days, with nearly 5 of those wetting the solid surfaces. The ion activity product (IAP) was calculated for the T7 liquid phase both before and after the test. Using the concentrations of calcium and oxalate ions in the liquid phase, it was calculated that the IAP pre-test is 9.21×10^{-7} $(\text{mol l}^{-1})^2$ and post-test is 2.07×10^{-7} $(\text{mol l}^{-1})^2$ assuming an activity coefficient of 0.28 for

urine calculated using the Davies and Guggenheim equations (Butler and Cogley 1998). The solubility product constant, K_{sp}, for calcium oxalate crystalline deposits is between 1.4×10^{-8} and 2.3×10^{-9} at 25°C (Vardhan and Generalic 2003). Therefore, since the IAP is higher than the K_{sp} throughout the duration of the test, the liquid phase was still supersaturated with calcium and oxalate ions. This explains the lack of precipitates observed, which likely would have increased with increased exposure time.

Some of the amorphous crystalline growth observed for T7 may have been the initial formation stages of the calcium oxalate crystals which would fully develop with further exposure. Stoichiometrically, only a third of the decrease in calcium ion concentrations can be attributed to calcium oxalates. Therefore, some of the deposits observed were potentially other calcium deposits or magnesium urates and phosphates as observed in other tests.

The amorphous and calcium oxalate deposits likely had a significant impact lowering θ_{adv} by virtue of their size. These crystals are generally smaller than 10 μm, much smaller than the liquid drops used to characterize θ_{adv}, which have an approximate radius of 2.26 mm. This fouling layer therefore provided a surface that is porous with microscopic roughness that promotes wetting and lowered θ_{adv}.

Impact of surface features

Surface roughness is another important parameter influencing contact angle, especially on a complex surface of crystals, biofilms, and other deposits. A Keyence VHX100 digital microscope was used to obtain three dimensional images of the fouled surfaces from which surface roughness and maximum defect height are extracted. A representative image from this procedure is shown in Figure 6.

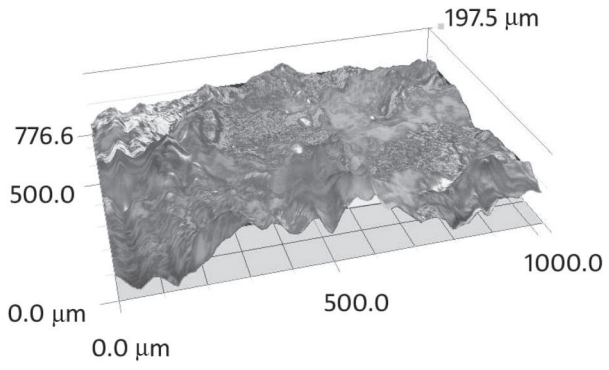

Figure 6. T5 representative VHX image.

In this study, surface roughness could not be isolated and quantified as a contributing factor to changes in θ_{adv}. First, the small crystals that lower θ_{adv} had a surface roughness comparable to the blank or only mildly fouled coupons, which had high θ_{adv}. Second, the larger features such as large struvite crystals, dried amorphous crystalline deposits, or dried biofilm presented relatively large pinning edges rather than more uniform surface roughness that tends to increase θ_{adv}. However, on these fouled surfaces, θ_{adv} was still influenced by the presence of biofilm and crystalline growth which lowered θ_{adv} below the baseline.

In lieu surface roughness, the maximum defect height observed in the VHX images was analyzed for significance. Defect height was used in ratio to capillary length, which was estimated to be a 2.26 mm radius for an 8 μl drop with $\theta_{adv} = 45°$. In Cubaud et al. (2001), defect width as a ratio to capillary length was combined with a term characterizing heterogeneity of the surface, where the defects were flush with the surface. In the present study, the defects were three dimensional, and heterogeneity was not directly accounted for as the surface energy of the complex fouling surfaces was not determined. The experimental data analyzed do not include the blank aluminum and ultem samples, because material selection confounded the results on the lesser fouled coupons. Also, the data of T6 aluminum were not considered due to extensive corrosion. θ_{adv} exhibited a significant linear dependence ($p = 0.0077$) on the ratio of defect height to capillary length, with a coefficient of 1192.9° mm/mm. Larger defect heights served to increase θ_{adv}, likely by creating pinning edges.

The tests where fouling layers consist of small crystal deposits exhibited defect heights ≈30 μm (approximately 1% of the capillary length). These rough and porous surfaces lowered θ_{adv} to ≈20°. In contrast, larger surface features ≈110 μm (approximately 5% of the capillary length) created pinning effects raising θ_{adv}. The average defect height was 68.7 μm (≈3% of the capillary length), and based on the linear regression, $\theta_{adv} = 36.3°$, less than the experimental average of 49.8°. These results indicate that defect height increased θ_{adv}, but less so than other fouling factors that lowered θ_{adv}.

Pretreatment

The impact of Oxone pretreatment chemicals added to the urine was isolated and analyzed. The results indicate that pretreatment had the potential to infrequently promote calcium oxalate deposits, which in turn lowered θ_{adv}. A more prevalent observation was amorphous crystalline deposits which grew in the

absence of pretreatment. Isolating the dataset apart from the occasional calcium oxalate presence reveals a significant influence of pretreatment ($p = 0.0001$), which raised θ_{adv} by approximately 15° to 35°.

The ascorbic acid in vitamin C is known to break down and produce oxalates promoting the development of calcium oxalate crystals (Stargrove et al. 2007). Therefore, it was presumed that Oxone oxidizes ascorbic acid in urine high in vitamin C content, converting it to oxalate and promoting the precipitation of calcium oxalate. As was shown with T7, calcium oxalate deposits may require several weeks to form precipitates. Additionally, other constituents in normal urine may promote or inhibit calcium oxalate growth and cannot always be predicted (Felix et al. 1976). Without pretreatment, magnesium urates and/or phosphates are promoted because uric acid and phosphates remain available for reaction and precipitation. Calcium oxalate deposits were not necessarily present on coupons exposed to urine pretreatment, while magnesium urates and phosphates were observed often in absence of pretreatment. Therefore, the general influence of pretreatment is to raise θ_{adv}.

Linear regression model

In hopes of employing the experimental results for the development of analytical tools for system design, an empirically based mathematical model was constructed to anticipate and interpret the impact of wastewater fouling on θ_{adv}. An imaging software program (MediaCybernetics' Image-Pro Analyzer) was employed to identify the percentage of homogenous 'smooth' regions of each ESEM image apart from complex features such as cracks and crystalline deposits to obtain fractional area coverage data. Fractional area fouling did not directly correlate to decreased θ_{adv} because of the counterbalancing effect of large pinning defects that increased θ_{adv}. However, fractional area fouling provided a reasonable approximation of surface fouling by biofilm and crystalline growth, both of which lowered θ_{adv}. A double linear regression was performed with both fractional area fouling (from the ESEM image processing) and largest defect height (observed in the three-dimensional VHX images).

The resulting linear model is in Equation (1), where f_{fouled} is the area fraction fouled, and d/l_{cap} is the ratio of defect height to capillary length, where the capillary length l_{cap} is the surface dimension over which surface tension forces are dominant. (Note: For small, surface tension-dominated droplets, the drop radius suffices for l_{cap}). This linear model correlates to the experimental data ($p < 0.001$). Figure 7 provides a comparison of Equation (1) with the experimental data used for the regression.

$$\theta_{adv} = 22.6 + 19.2 f_{fouled} + 1256.3 \frac{d}{l_{cap}} - 1138 \left(f_{fouled} \frac{d}{l_{cap}} \right)$$
$$\text{for} \left\{ 0 \le f_{fouled} \le 10 \le \frac{d}{l_{cap}} \le 0.12 \right\}$$
$$\text{such that } 0^\circ \le \theta_{adv} \le 180^\circ \quad (1)$$

Equation (1) implies that a clean surface with no defects yields the lowest θ_{adv}, though this does not correspond to the blank titanium coupon, wherein surface defects were observed on the order of 50 μm. The lowest θ_{adv} observed was on completely fouled coupons with small surface defects, and the highest θ_{adv} was on minimally fouled surfaces with large defects.

The empirically developed Equation (1) supports the interpretation that wastewater fouling will generally decrease θ_{adv} from the baseline on a clean but imperfect surface. The average defect height was 68.7 μm (approximately 3% of the capillary length) while the average areal coverage was over 60%. Using Equation (1), these means correspond to θ_{adv} of 51.3°, which is only 3% in discrepancy from the experimental average value of 49.8°, which is itself about 20° less than the clean titanium surface baseline. The model has a mean error of ≈40% from the experimental data, with a SD of ≈27%. As observed in Figure 7, many of the data points fall close to the model contour lines for the range of experimental points ($0.001 \le f_{fouled} \le 0.961$, $0.009 \le d/l_{cap} \le 0.117$), while some fewer points do not agree well with the model. In the absence of more precise tools, this model may be used as a preliminary guide for impact of fouling on contact angle.

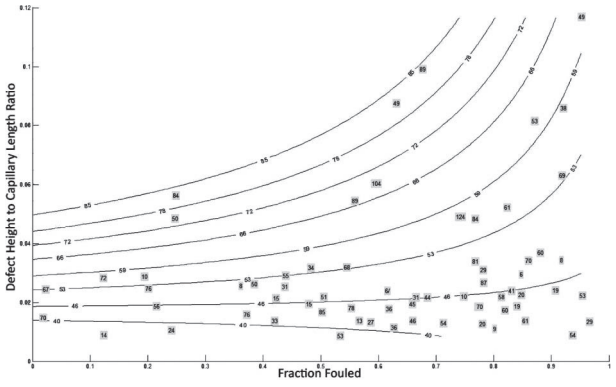

Figure 7. Comparison of θ_{adv} from Equation (1) (contour lines) with experimental data (shaded boxes) for give ranges ($0.001 \le f_{fouled} \le 0.961$, $0.009 \le d/l_{cap} \le 0.117$).

Equation (1) does not directly take into account surface energy changes, heterogeneity, porosity or roughness, as each of these parameters was difficult to estimate independently. However, to a degree, areal coverage represents a combined effect of these parameters, while defect height accounts in part for the significant influence of pinning edges. In categorizing the significant influences on θ_{adv}, areal coverage groups crystalline deposits, biofilm growth, and magnesium concentration influences, while defect height accounts for large surface features and vacuum drying influences that create pinning edges.

Summary

Calcium oxalate crystal deposits, amorphous minerals deposits including magnesium urates and/or phosphates, and biofilm growth all lowered the DI water advancing contact angle θ_{adv} by as much as 64°, while the crystals lowered θ_{adv} more substantially than biofilm. Fouling surface defects $>5\%$ of the capillary length increased θ_{adv} by as much as 43°. Vacuum drying of fouled coupons increased θ_{adv} by as much as 13°. For the complete dataset, the average θ_{adv} was approximately equal to the pretest baseline value. For example, test T9, which was most similar to the expected operational conditions for the target spacecraft SPS technology, showed crystalline and biofilm growth as well as large defects, resulting in an overall average θ_{adv} of 69.4°, effectively identical to the baseline 69.7°.

The current experiments approximately isolated several wastewater fouling characteristics and their impact on θ_{adv}, a property of any capillary system. Vacuum drying and large defects increased θ_{adv}, while crystal and biofilm growth lowered θ_{adv}. The use of Oxone as a pretreatment generally increased θ_{adv}. This study does not examine direct causes of wastewater fouling, but rather provides insight into the general trends of wastewater fouling on θ_{adv}. The trends indicate that promotion of wastewater fouling may significantly decrease θ_{adv} and thereby improve the performance of capillary-based fluid management systems.

Acknowledgements

The authors thank colleagues at the NASA-Johnson Space Center, including K. Pickering, C. Carrier, N. Adam, M. Nelman, A. Almengor, M. Casteel, J. Graf, and O. Estrada.

References

APHA. 2006. Standard Methods for the Examination of Water and Wastewater. Online Edition www.standardmethods.org. Washington (DC): American Public Health Association, American Water Works Association, Water Environment Federation.

Bico J, Tordeux C, Quere D. 2001. Rough wetting. Europhys Lett 55:214–220.

Brizzolara R, Holm E. 2006. The effect of solid surface tension and exposure to elevated hydrodynamic shear on *Pseudomonas fluorescens* biofilms grown on modified titanium surfaces. Biofouling 22:431–440.

Brunzel N. 2004. Fundamentals of urine and body fluid analysis. 2nd ed. St Louis (MO): Elsevier Health Sciences.

Butler J, Cogley D. 1998. Ionic equilibrium: solubility and pH calculations. 2nd ed. Maiden (MA): Wiley-Interscience.

Comper W, Jerums G, Osicka T. 2004. Differences in urinary albumin detected by four immunoassays and high-performance liquid chromatography. Clin Biochem 37: 105–111.

Cooksey KE. 1992. Extracellular polymers in biofilms. In: Melo L, editor. Biofilms – science and technology. Dordrecht (NL): Kluwer Academic Publishers. p. 137–145.

Cubaud T, Fermigier M, Jenffer P. 2001. Spreading of large drops on patterned surfaces. Oil Gas Sci Technol 56:23–31.

Dodge F. 2000. The new dynamic behavior of liquids in moving containers. San Antonio (TX): Southwest Research Institute.

Donlan RM. 2002. Biofilms: microbial life on surfaces. Emerg Infect Dis 8:881–890.

Doyle J, Parsons S. 2002. Struvite formation, control and recovery. Water Res 36:3925–3940.

Dyson D. 1988. Contact line stability at edges: comments on Gibbs's inequalities. Phys Fluids 31:229–232.

Felix R, Monod A, Broge L, Hansen N, Fleisch H. 1976. Aggregation of calcium oxalate crystals: effect of urine and various inhibitors. Urol Res 5:21–28.

Fletcher M. 1992. Bacterial metabolism in biofilms. In: Melo L, editor. Biofilms – science and technology. Dordrecht (NL): Kluwer Academic Publishers. p. 113–119.

Metrohm. 2008. Metrohm ion analysis 850 professional IC manual (cation and anion). Herisau (CH): Metrohm AG.

NASA-JSC. 2008. CxP 70000 Constellation architecture requirements revision B. Houston (TX): NASA-Johnson Space Center.

Oliveira DR. 1992. Physico-chemical aspects of adhesion. In: Melo L, editor. Biofilms – science and technology. Dordrecht (NL): Kluwer Academic Publishers. p. 45–57.

Schmitt J, Flemming H-C. 1998. FTIR-spectroscopy in microbial and material analysis. Int Biodeterior Biodegr 41:1–11.

Schneider R, Ferreira L, Binder P, Ramos J. 2005. Analysis of foulant layer in all elements of an RO train. J Membr Sci 261:152–162.

Sharma P, Hanumantha R. 2002. Analysis of different approaches for evaluation of surface energy of microbial cells by contact angle goniometry. Adv Colloid Interface Sci 98:341–463.

Simoes M, Pereira M, Sillankorva S, Azeredo J, Vieira M. 2007. The effect of hydrodynamic conditions on the phenotype of *Pseudomonas fluorescens* biofilms. Biofouling 23:249–258.

Stargrove M, Treasure J, McKee D. 2007. Herb, nutrient, and drug interactions. St Louis (MO): Elsevier Health Sciences.

Strasinger S, DiLorenzo M. 2001. Urinalysis and body fluids. 4th ed. Philadelphia (PA): F.A. Davis Company.

Udert K, Larsen K, Gujer W. 2003. Biologically induced precipitation in urine-collecting systems. Water Sci Technol: Water Supply 3:71–78.

Vardhan A, Generalic E, Solubility product constants [Internet]. 2003. Split (HR): Faculty of Chemistry and Technology; [cited November 18, 2008]. Available from: http://www.ktf-split.hr/periodni/en/abc/kpt.html.

Wallace L, Campbell M. 2005. Urine pre-treatment assessment: technology development plan. Houston (TX): Lockheed Martin Space Operations.

Weislogel M, Thomas E, Graf J. 2008. A novel device addressing design challenges for passive fluid phase separations aboard spacecraft. J Microgravity Sci Technol, DOI: 10.1007/s12217-008-9091-7, 6 August 2008. Available at http://www.springerlink.com/content/u1616h27k45v8310/.

Whitson P, Pietrzyk R, Pak C. 1997. Renal stone risk assessment during space shuttle flights. J Urol 158: 2305–2310.

Whitson P, Pietrzyk R, Morukov B, Sams C. 2001. The risk of renal stone formation during and after long ruration space flight. Nephron 89:264–270.

Winkler H, Verostko C, Dehner G. 1983. Urine pretreatment for wastewater processing systems (no. 831113). San Francisco (CA): SAE Technical Paper Series.